

Axisymmetric Pushing of a Spherical Cargo using an Active Spherical Janus Motor

Subramaniam Chembai Ganesh,¹ Jessica S. Rosenberg,² Jeffrey F. Morris,¹ Joel Koplik,² and Charles Maldarelli¹

¹*Benjamin Levich Institute and Department of Chemical Engineering, City College of the City University of New York, New York, New York 10031, USA*

²*Benjamin Levich Institute and Department of Physics, City College of the City University of New York, New York, New York 10031, USA*

(Dated: January 22, 2025)

We analyze the interaction between a self-diffusiophoretic spherical Janus motor and an inert spherical cargo particle in an axisymmetric configuration in the Stokes regime. To study the different configurations of the two spheres and their motions, we develop an analog to the twin multipole approach to numerically determine the axisymmetric stream function for the flow field. We verify the validity and accuracy of this approach using existing literature and COMSOL Multiphysics. We study the effects of the size of the Janus cap, the relative ratio of sizes of the two spheres, and their separation distance on their interactions. For the case of a stationary cargo, we identify the existence of a distinct regime where the Janus motor hovers at a finite separation distance from the cargo and summarize the results using a phase diagram. In the presence of a freely moving cargo, we analyze the steady terminal velocities of the Janus motor and the cargo to identify distinct conditions at which the two spheres can translate with equal velocities while maintaining a finite separation distance.

I. INTRODUCTION

The study of microscopic self-propelled particles ('swimmers') is of interest due to their relevance in natural biological systems [1], targeted drug delivery [2], [3], medical diagnostics [4] and for their ability to self-assemble [5]. These swimmers typically operate in the low Reynolds number regime where the absence of inertia requires that the net propulsion of any particle at this scale with moving parts must employ a mechanism that breaks time symmetry [6]. We study Janus motors (JMs) which are Janus particles whose surfaces are functionalized to interact asymmetrically with the surrounding environment to generate the necessary propulsion forces for their motion. One such self-propulsion mechanism is the well studied Self-diffusiophoresis. Here, the chemically active JM reacts enables the asymmetric efflux of some solute, creating a local concentration gradient that drives its motion [7], [8], [9], [10]. Spherical JMs (typically in the range of 1-10 microns) have been studied both in an infinite medium both experimentally [11], [12], [13], [14] and theoretically [15], [16], [17] (For review see [18], [19], [20], [21]).

To understand the dynamics of JMs for applications such as colloidal assembly [5], or cargo towing [22], it is essential to understand the interaction of JMs among themselves or with other particles/obstacles. In an effort to simplify the analysis for the general interactions involving JMs, there have been many efforts in recent literature to understand the pair interactions of JMs and JMs with other particles [23], [24], [25], [26], [27]. Baraban et al. 2012 [23] experimentally studied the interaction between JMs with varying activities on their surfaces and (inert) cargo particles. They used polystyrene particles coated with platinum placed in an aqueous solution of hydrogen peroxide. The platinum cap on the JM catalyses the decomposition of the hydrogen peroxide in the solution to create a concentration gradient of oxygen around the JM, thereby driving its motion. Baraban et al. found that when a single JM with a hemispherical active cap collides with the cargo, it can allow continued pushing; showing a kind of towing.

While complete theoretical studies of cargo towing haven't been undertaken, there have been studies of the interaction between JMs. Sharifi-Mood et al. 2016 studied pairs of two JMs using the Reynolds Reciprocal Theorem [28], [29] to solve for the terminal velocities of the particles. They studied different configurations of the two JMs; including how different orientations between the active faces, sizes of the active faces, and distances between the two JMs affected their motion. Their research concluded with a phase diagram that makes explicit the effects of these variables, and whether they lead to approach, assembly or the two particles moving apart.

Golestanian et al. studied axisymmetric JMs in pairs. They made use of bispherical coordinates [30] to fully solve for the forces, torques, as well as the self-diffusiophoretic slip velocity on the JM's surface. They created generic geometric functions that can be summed to find the relative velocity of the two particles and exposes the effect that the JM's activity has on the analytical solution. While Golestanian et al. and Sharifi-Mood both look at two JMs, the focus of our study is to develop a more complete description of the of the axisymmetric interaction between a JM and an inert cargo with emphasis on the cargo-towing application. In our paper we apply the twin multipole approach [31] to solve the hydrodynamic axisymmetric stream function. The twin multipole approach has been popularized by Jeffrey [32] who solved the temperature field for the conduction of heat in the presence of two particles and later

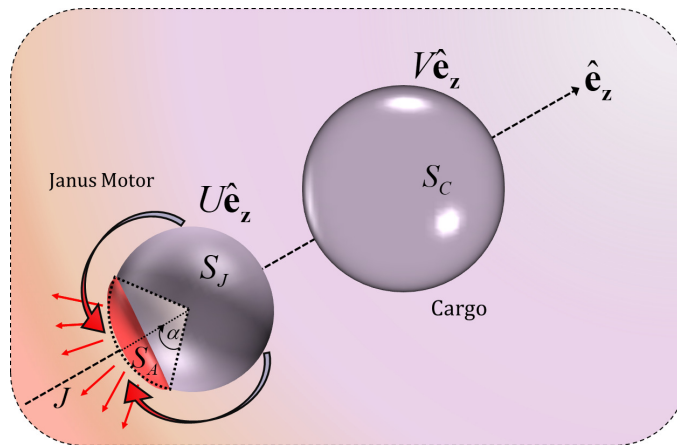


FIG. 1: A JM and cargo in an axisymmetric configuration moving with velocities $U\hat{e}_z$ and $V\hat{e}_z$ respectively. The flux of the solute is indicated by J , the cap angle by α along a meridional plane.

by [33] for the hydrodynamic interactions between two spheres, where the solutions could be described by spherical harmonics. The novelty of our approach comes from extending the technique to the axisymmetric stream function which does not satisfy the harmonic equation. Further, the twin multipole approach employs relatively straightforward spherical coordinates for solving the governing equations. This allows for simpler application of boundary conditions, and easier evaluation of quantities of interest (such as stress fields and net forces) compared to more complex solution techniques such as using a bispherical basis etc.

II. PROBLEM STATEMENT

We consider an active spherical JM of radius R_1 and an inert spherical cargo of radius R_2 immersed in a liquid of density $\rho(\frac{kg}{m^3})$ and viscosity $\mu(\frac{kg}{ms})$. We limit our discussions to the axisymmetric configuration where the vector pointing to the cargo's center from the center of the JM is parallel to \hat{e}_z .

The size of the active cap \mathbf{S}_A of the JM is represented by the angle defined with respect to \hat{e}_z along any meridional plane as shown in Figure 1 and indicated by α . We assume the active cap produces a constant flux of magnitude, $J(\frac{mol}{m^2s})$ of some solute in the normal direction to its surface. The remaining portion of the JM, \mathbf{S}_J and the entire cargo, \mathbf{S}_C are both inert (no flux). A local gradient of solute concentration $C(\frac{mol}{m^3})$ created by the difference in chemical properties on the JM's face induces an osmotic flow along the surface of the JM [7] which propels the motor and the cargo with terminal velocities $U\hat{e}_z$ and $V\hat{e}_z(\frac{m}{s})$ respectively.

We assume the solute has a diffusion coefficient $D(\frac{m^2}{s})$ in the surrounding fluid, so we can define the dimensionless Péclet number $Pe = UR_1/D$ and the Reynolds number $Re = \rho UR_1/\mu$ for the problem, using the radius (R_1) and velocity (U) of the JM as our characteristic length and velocity scales respectively.

III. CONCENTRATION FIELD

We assume our concentration field of the solute is purely diffusive ($Pe \rightarrow 0$). Therefore the field is governed by the Laplace equation,

$$\nabla^2 C = 0. \quad (1)$$

Since the presence of any constant ambient concentration of the solutes far away does not affect the gradients in the concentration field, We can also assume that the concentration field decays to zero far field, giving us the corresponding boundary conditions,

$$C \rightarrow 0 \quad \{\mathbf{x} \rightarrow \infty\}, \quad (2)$$

$$\hat{\mathbf{n}} \cdot \nabla C = 0 \quad \{\mathbf{x} \in \mathbf{S}_C, \mathbf{S}_J\}, \quad (3)$$

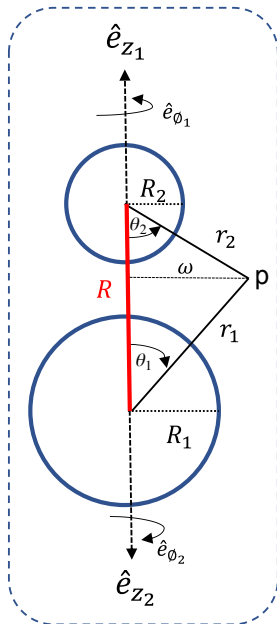


FIG. 2: Description of the two basis systems used for the twin multipole approach.

$$\hat{\mathbf{n}} \cdot \nabla C = \frac{-J}{D} \quad \{\mathbf{x} \in \mathcal{S}_A\}. \quad (4)$$

We nondimensionalize equations 1, 2, 3, 4 by length R_1 , implying a natural scale of JR_1/D for the concentration field.

We implement the twin multipole approach to solve for the concentration field. Here, we write the solutions to the concentration field as the sum of two concentration fields $C = C_1 + C_2$ using two spherical coordinate systems (r_1, θ_1, ϕ_1) (r_2, θ_2, ϕ_2) with their origins at the center of the JM and cargo respectively as shown in Figure 2. The two fields satisfy the governing equation 1. We can then write the general solutions as an expansion in solid harmonics that decay to zero at infinity (from 2).

$$C = \sum_{i=1}^2 C_i = \sum_{i=1}^2 \sum_{n=0}^{\infty} \left[(B_i)_n r_i^{-(n+1)} \right] p_n(\gamma_i) \quad \forall \{\gamma_i = \cos\theta_i\}, \quad (5)$$

where p_n is the n^{th} order Legendre polynomial function. We then apply boundary conditions 2, 3, 4 using the translation theorem,

$$\frac{P_n(\cos\theta_2)}{r_2^{n+1}} = \sum_{m=0}^{\infty} \binom{m+n}{n} \left(\frac{r_1^m}{R^{m+n+1}} \right) P_m(\cos\theta_1). \quad (6)$$

Equation 6 is useful because the boundary conditions can be applied on the JM and by interchanging the indices 1, 2, the boundary conditions can be applied on the cargo. The unknown coefficients $(B_1)_n$, $(B_2)_n$ can be solved for simultaneously by numerically inverting the resulting system of equations.

IV. VELOCITY FIELD

In problems involving neutral diffusiophoresis, the flow field is typically assumed to be inertia-less ($Re \rightarrow 0$) [25, 27] and the velocity, \mathbf{u} and pressure p fields are governed by the incompressible Stokes equations

$$-\nabla p + \mu \nabla^2 \mathbf{u} = 0, \quad (7)$$

$$\nabla \cdot \mathbf{u} = 0. \quad (8)$$

The corresponding boundary conditions are

$$\mathbf{u} = 0 \quad \{x \rightarrow \infty\}, \quad (9)$$

$$\mathbf{u} = U\hat{\mathbf{e}}_z + \beta\nabla_s C \quad \{x \in S_C, S_J\}, \quad (10)$$

$$\mathbf{u} = V\hat{\mathbf{e}}_z \quad \{x \in S_C\}. \quad (11)$$

Where β is the diffusiophoretic slip coefficient which has positive values when the interaction between the JM and the solute is repulsive, $\hat{\mathbf{n}}$ is the normal unit vector pointing into the fluid from the solid surfaces and $\nabla_s = (\boldsymbol{\delta} - \hat{\mathbf{n}}\hat{\mathbf{n}}) \cdot \nabla$. Since there are no external forces, the net force on the cargo ($F_C^{net} \hat{\mathbf{e}}_z$) and the JM ($F_J^{net} \hat{\mathbf{e}}_z$) are equal to zero.

$$F_J^{net} \hat{\mathbf{e}}_z = \iint_{S_J, S_A} (\hat{\mathbf{e}}_z \cdot \boldsymbol{\sigma} \cdot \hat{\mathbf{n}}) ds = 0 \quad (12)$$

$$F_C^{net} \hat{\mathbf{e}}_z = \iint_{S_C} (\hat{\mathbf{e}}_z \cdot \boldsymbol{\sigma} \cdot \hat{\mathbf{n}}) ds = 0 \quad (13)$$

where $\boldsymbol{\sigma}$ is the Cauchy stress tensor. We can use the Stokes stream function to simplify the calculations given the axisymmetric nature of the problem. We define the velocity field in terms of the stream function,

$$\mathbf{u} = \nabla \times \left(\frac{\boldsymbol{\Psi}}{\omega} \right). \quad (14)$$

The stream function satisfies the linear equation $\nabla \times \nabla \times \nabla \times \nabla \times \left(\hat{\mathbf{e}}_\phi \frac{\psi}{\omega} \right) = E^4 \psi = 0$. We use a twin multipole approach to solve for the stream function. The eigenfunction expansion for the stream function for an unbounded fluid can be written using the two spherical coordinates defined in Figure 2 as

$$\boldsymbol{\Psi} = \sum_{i=1}^2 \psi_i \hat{\mathbf{e}}_{\phi_i} = \sum_{i=1}^2 \sum_{n=1}^{\infty} \left[(X_i)_n r_i^{2-n} (Y_i)_n r_i^{-n} \right] g_n(\cos\theta_i) \hat{\mathbf{e}}_{\phi_i}. \quad (15)$$

Here, the eigenfunctions are defined in terms of the modified Gegenbauer polynomials $g_n(\gamma) = -\mathbb{C}_{n+1}^{-1/2}(\gamma)$ [34]. Note, the vector sum of the stream function gives us $\boldsymbol{\Psi} = (\psi_1 - \psi_2) \hat{\mathbf{e}}_{\phi_1} = (\psi_2 - \psi_1) \hat{\mathbf{e}}_{\phi_2}$. We now rewrite the boundary conditions 9, 10, 11 in terms of the stream functions and satisfy these boundary conditions on the surface of the spheres using the following translational theorems

$$\frac{g_n(\gamma_2)}{r_2^n} = \sum_{m=0}^{\infty} \left(\frac{R_1^m}{2n+1} \right) \left[\Omega_1 p_m(\gamma_1) + \Omega_2 p_{m-1}(\gamma_1) + \Omega_3 p_{m+1}(\gamma_1) \right], \quad (16)$$

$$\frac{g_n(\gamma_2)}{r_2^{n-2}} = \sum_{m=0}^{\infty} \left(\frac{R_1^m}{2n+1} \right) \left[\Omega_4 p_m(\gamma_1) + \Omega_5 p_{m-1}(\gamma_1) + \Omega_6 p_{m+1}(\gamma_1) + \Omega_7 p_{m-2}(\gamma_1) + \Omega_8 p_{m+2}(\gamma_1) \right]. \quad (17)$$

We define the functions $\Omega_1(r_1, r_2, R)$ through $\Omega_8(r_1, r_2, R)$ in Appendix ???. The following identities are useful in applying the boundary conditions.

$$g_n(x) = \frac{p_{n+1}(x) - p_{n-1}(x)}{2n+1} \quad (\text{Bonnet's recursion theorem}), \quad (18)$$

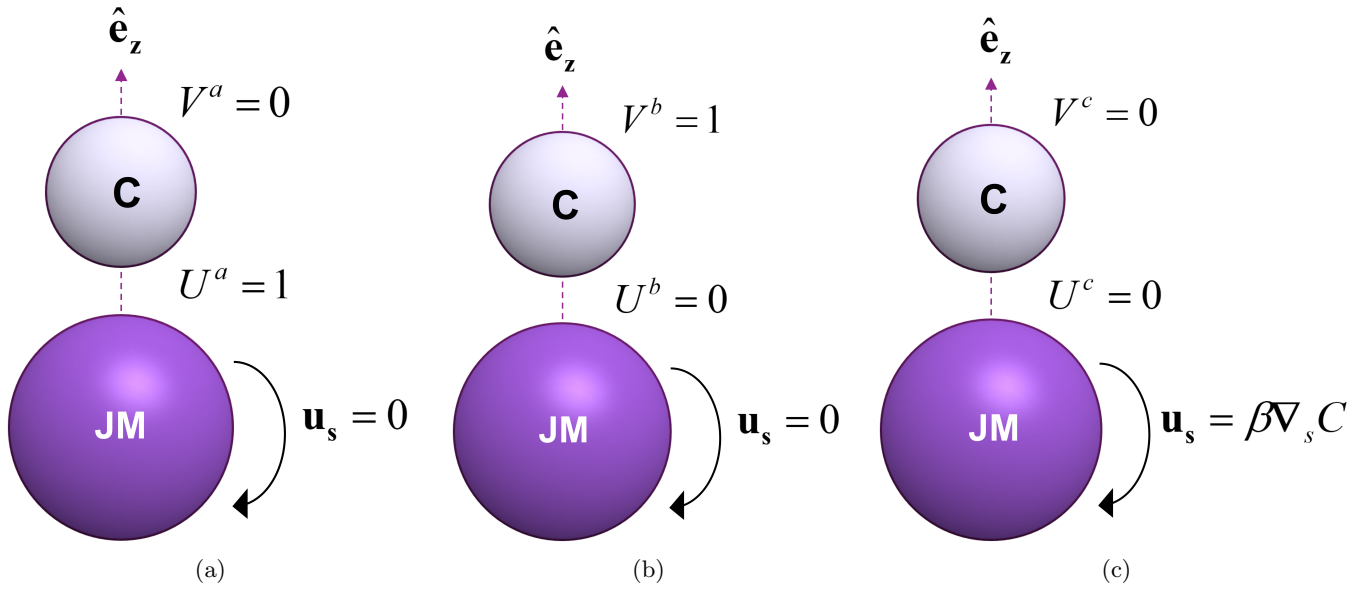


FIG. 3: 3a represents the sub-problem in which only the JM has translational velocity. 3b shows the case in which only the cargo has translational velocity. Finally, 3c shows the problem where neither particle has any translational velocity and there is only a slip velocity, \mathbf{u}_s , prescribed on the JM's surface due to diffusiophoresis.

$$\frac{d}{dx}g_n(x) = p_n(x). \quad (19)$$

Since Stokes flow is linear, we split the net force on each particle into three sub-forces respectively; $F^{net} = (UF^a + VF^b + F^c)\hat{\mathbf{e}}_z$ each of which corresponds to the three sub-problems described in Figure 3. We use superscripts to differentiate the sub-problems. We will refer to the force due to sub-problem 3 (Figure 3c) with the slip velocity as the propulsion force since this force drives the JM and the cargo. The other two forces correspond to the velocity dependent hydrodynamic drags that balance the propulsion force.

The boundary conditions 9, 10, 11 can be rewritten in terms of the stream functions, and like the concentration field, can be split into the three sub-problems. These boundary conditions can then be applied to the general solution 15 to obtain a coupled system of equations which we can then numerically invert for the coefficients

$X_{1n}^j, X_{2n}^j, Y_{1n}^j, Y_{2n}^j, j \in \{a, b, c\}$ for each sub-problem.

Finally, we can calculate the propulsion forces for both spheres either by integrating the stress tensor corresponding to sub-problem 3 (Figure 3c) about the surface of the two spheres as defined in Equations 12 and 13 or by using the reciprocal theorem [28] which relates the forces F^c to the stress fields σ^a, σ^b

$$F_J^c \hat{\mathbf{e}}_z = \iint_{S_J, S_A} (\hat{\mathbf{e}}_z \cdot \sigma^a \cdot \hat{\mathbf{n}}) ds, \quad (20)$$

$$F_C^c \hat{\mathbf{e}}_z = \iint_{S_J, S_A} (\hat{\mathbf{e}}_z \cdot \sigma^b \cdot \hat{\mathbf{n}}) ds. \quad (21)$$

The advantage of using the latter approach is that we can directly calculate the propulsion forces from the stress tensors of sub-problems 1 and 2 (Figures 3a and 3b) which have already been well studied in literature [33, 35]. Note that the integrals in 20 and 21 are only over the surface of the JM. Finally, we reduce the force free conditions in Equations 12 and 13 to Equation 22

$$\begin{bmatrix} F_J^a & F_J^b \\ F_C^b & F_C^a \end{bmatrix} \begin{bmatrix} U \\ V \end{bmatrix} = \begin{bmatrix} -F_J^c \\ -F_C^c \end{bmatrix}. \quad (22)$$

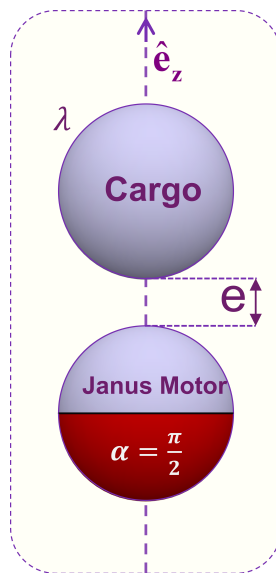


FIG. 4: An illustration of a JM and a cargo with $\alpha = \pi/2$.

V. RESULTS AND DISCUSSION

We define the size of the cargo relative to the JM (R_1) as $\lambda = R_2/R_1$. We also define a scaled edge-to-edge separation as $e = R/R_1 - (1 + \lambda)$. The results are evaluated by truncating the concentration field 5 and stream functions 15 to 100 terms in and using the first 25 terms of the stream function expansion to evaluate the forces on the JM and the cargo by integrating the stress on each sphere for each sub-problem. The forces presented in this section are scaled by a factor of $\frac{6\pi\mu\beta J R_1}{D}$ and the terminal velocities are presented scaled by a factor of $\frac{\beta J}{D}$. The twin multiple approach is singular at the limit of $e \rightarrow \infty$ [33] so we limit the closest approach in our results to $e = 0.1$.

A. Stationary Cargo

In Figure 5 we consider the propulsion forces for $\lambda = 1, 2$ and 5 for 3 different cap sizes $\alpha = \frac{\pi}{2}, \frac{6\pi}{7}$ and $\frac{9\pi}{10}$. For sufficiently small values of α , the force on the JM and the cargo are towards each other and above a certain stagnant cap size, the JM and the cargo exhibit a reversal of the direction of propulsion. To understand the reason, it is necessary to take a look at the concentration field of the produced solute. Figure 6 shows the concentration field and the direction of concentration gradients on the surface of the JM for select separation distances and Figure 7 shows the corresponding flow field and streamlines. It is evident that under select circumstances that depend on (α, λ, e) , the concentration of solutes exhibits a non monotonic behavior along the surface of the JM. The accumulation of solutes at closer separations in between the JM and the cargo lead to a reversal of the direction of the tangential concentration gradient on it's surface. This leads to opposing slip velocities along the JM surface from 10 creating competing contributions to the propulsion forces as the corresponding flow from sub-problem 3 (3c) is purely driven by slip velocity.

If the cargo is held stationary (I.e. $V = 0$), then the resulting velocity of the Janus particle can be directly found from the force free condition 12 which simplifies to $U = -\frac{F_J^c}{F_J}$. The JM velocity $U = 0$, if $F_J^c = 0$. Therefore, if the propulsion force on the JM vanishes for a given configuration of (λ, α) at a fixed separation distance $e = e_h$, the JM is considered to be "hovering" at this fixed position with respect to the cargo. The concentration field still generates a flow due to the slip on the surface of the JM creating a flow field around the two spheres. Note that since the cargo is held stationary, it can still experience a force from this flow (I.e. $F_C^c \neq 0$) as seen from the different x intercepts of the two forces in Figure 8. Upon inspecting the direction of the forces in the hovering configurations, it is evident that the hovering state is stable to translational perturbations of the JM along the line of centers. Further study is necessary to confirm the stability of the hovering configuration to non-axisymmetric perturbations.

Figure 8 shows that when increasing α keeping λ fixed, the hovering separation distance e_h also increases as expected given that the larger stagnant cap size reduces the asymmetry in the distribution of the solute around the JM. Therefore, a lesser extent of accumulation of the solute between the JM and the cargo can cause opposing

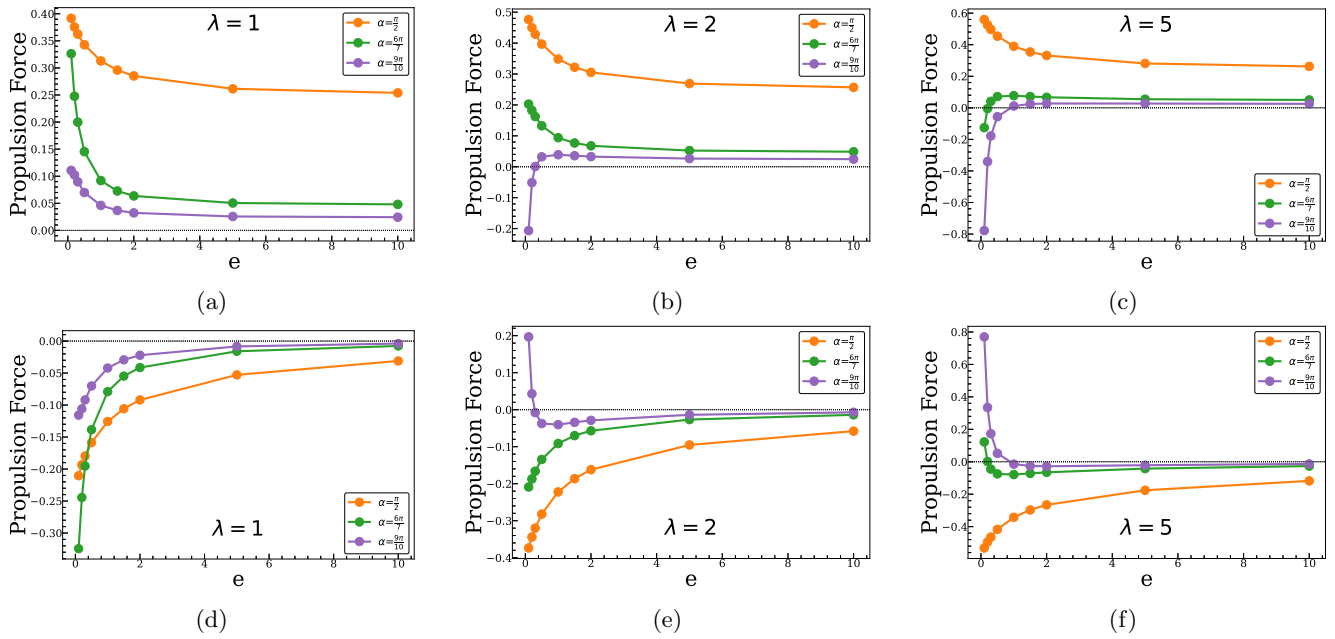


FIG. 5: Propulsion forces for the JM (a,b,c) and the cargo (d,e,f) with $\alpha = \frac{\pi}{2}, \frac{6\pi}{7}, \frac{9\pi}{10}$ and $\lambda =$ (a,d) 1, (b,e) 2 and (c,f) 5.

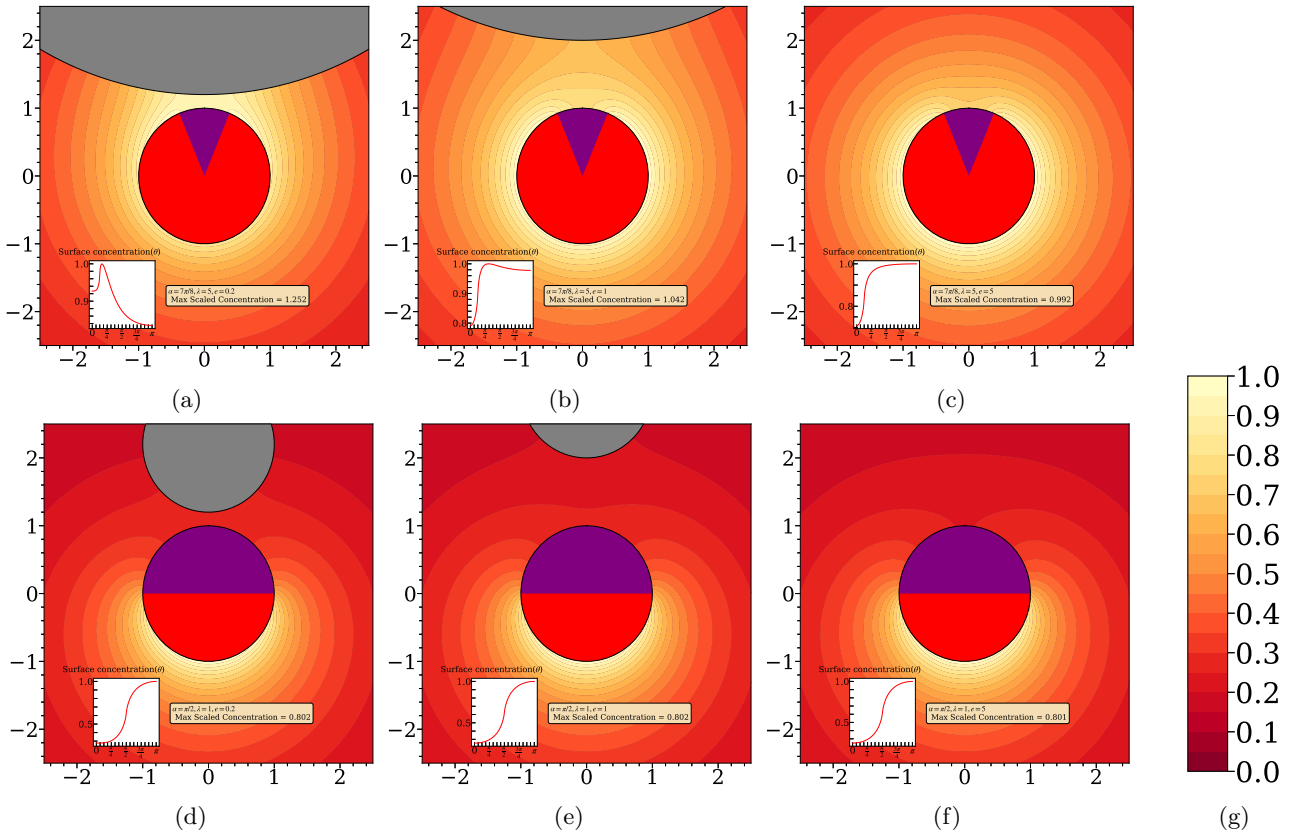


FIG. 6: Normalized concentration fields (with an inset of surface concentration along the JM's surface) for the JM and the cargo with $(\lambda = 5, \alpha = \frac{7\pi}{8})$ at $e =$ (a) 0.2, (b) 1, (c) 5 and for $(\lambda = 1, \alpha = \frac{\pi}{2})$ at $e =$ (d) 0.2, (e) 1, (f) 5.

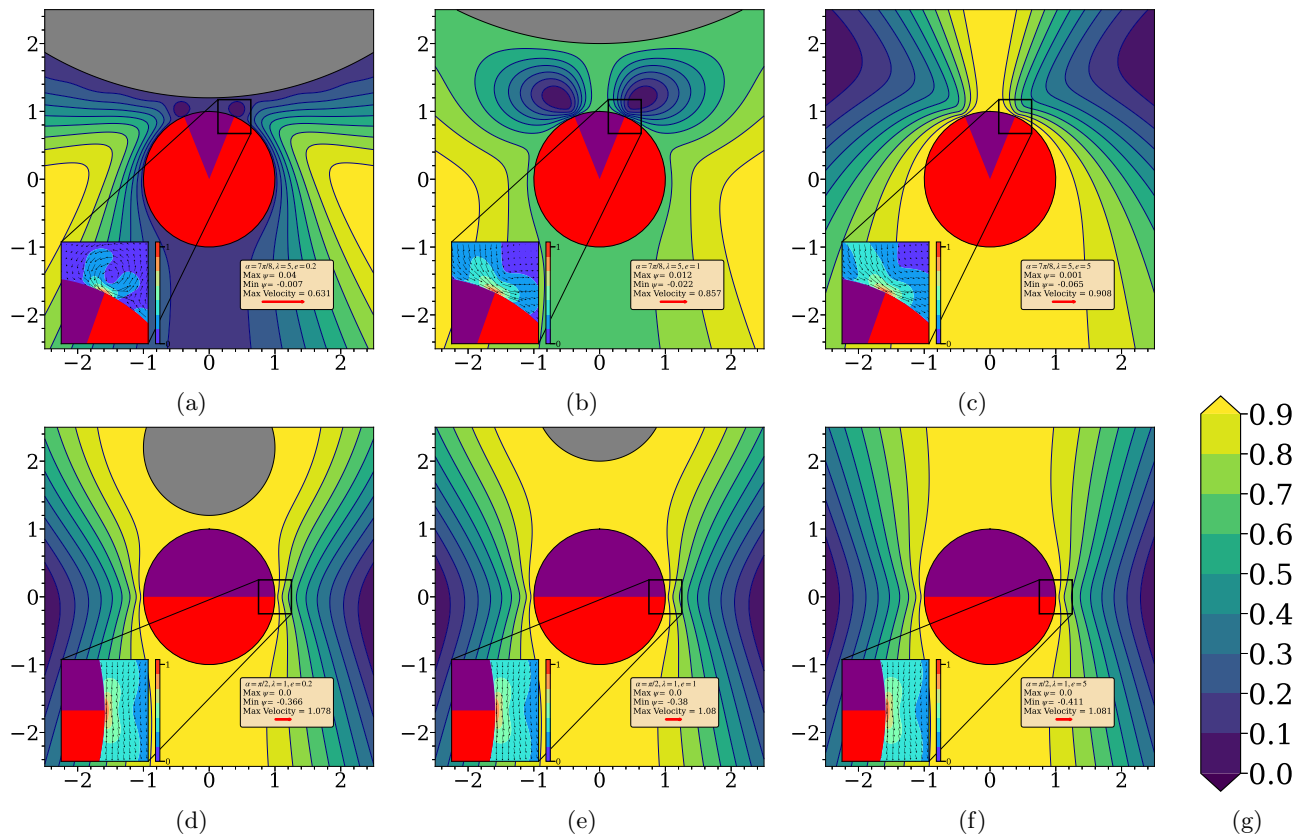


FIG. 7: Normalized streamlines and velocity fields for the JM and the cargo with $(\lambda = 5, \alpha = \frac{7\pi}{8})$ at $e =$ (a) 0.2, (b) 1, (c) 5 and for $(\lambda = 1, \alpha = \frac{\pi}{2})$ at $e =$ (d) 0.2, (e) 1, (f) 5.

tangential concentration gradients on the surface of the JM leading to opposing slip velocities that allow the JM to hover at further distances from the cargo.

by the corollary, the hovering separation decreases with decreasing α and there exists a minimum cap size (α_{min}) for a given (λ) where $e_h \rightarrow 0$. For $\alpha < \alpha_{min}$, the JM will tend to crash into the cargo if not for lubrication effects.

When we increase λ , the minimum cap angle required to allow hovering α_{min} reduces, as can be seen by looking at Figure 5. Hence, there exists a global minimum, α_{min} that corresponds to the case where $\lambda \rightarrow \infty$ that is physically equivalent to the case of a JM normally approaching a planar wall. This problem has been studied in detail by [36] where the authors showed that the JM can hover over a wall at a minimum stagnant cap angle of about $\alpha_{min} \approx 145^\circ$

In the limit of $e \rightarrow \infty$, the propulsion force on the cargo goes to zero. In this limit the JM experiences a propulsion force which approaches the value of a single JM at infinite separation here. For the JM to hover at infinite separation, the active cap must cover the entire motor so that the resulting asymmetry in the concentration field vanishes. In other words, as $e \rightarrow \infty$, $\alpha_{min} \rightarrow \pi$.

Based on these observations, we create a phase diagram that predicts the existence of the hovering point in the trajectory of approach of the JM to the cargo. Figure 9a depicts the proposed phase diagram with illustrations of the various configurations that the two spheres sustain at steady state. Since, we do not have an analytical solution to the minimum cap size for a given size ratio (I.e. $\alpha_{min}(\lambda)$), we can use an extrapolation approach to approximate the same. For a given λ , we estimate the hovering separation distance (e_h) to within ± 0.005 by seeking a change in sign of the force on the JM with systematic increments of e . We then use a bi quadratic polynomial to generate a least squares fit of e_h as a function of α . We can then predict α_{min} by extrapolating the fitted polynomial to $e_h = 0$. Plots of the fitted polynomial for $\frac{1}{\lambda} = 0.2, 0.5, 1$ and 1.5 are shown in Figure 9b. Plotting the predicted α_{min} with respect to $\frac{1}{\lambda}$, we can approximate the phase boundary of the possible configurations (α, λ) where the JM and the stationary cargo can experience a hovering state (Figure 9c). We can use a similar approach to interpolate the required α for any e_h . Figure 9c also shows lines of constant hovering separation distances $e_h = 0.5, 1, 1.5$. We can further use a similar polynomial fitting to extrapolate the generated iso-separation lines and the phase boundary to the limiting case of $\lambda \rightarrow \infty$ (I.e., the x intercepts in Figure 9c) to compare with the existing literature on hovering of JM near a planar wall from [36] (Figure 9d. where in spite of the double extrapolation, there is a reasonable agreement. Note, in

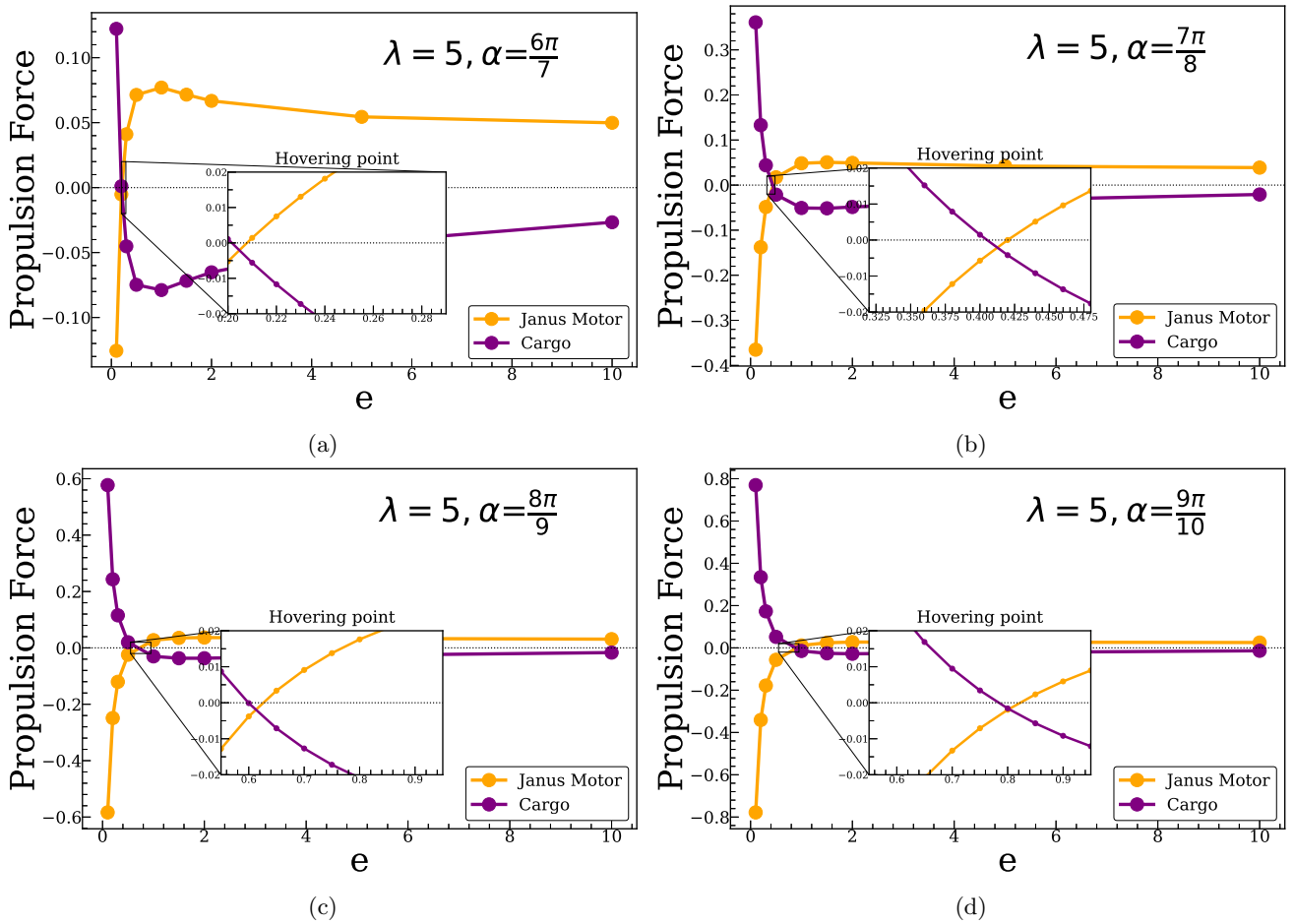


FIG. 8: Plots of the propulsion forces on the JM and the cargo for $\lambda = 5$ depicting the monotonic increase of hovering separation distance (e_h) with increasing stagnant cap angles (α).

Figure 9, the data points are plotted along with their corresponding polynomial fits (dotted lines) whereas in the plots depicting the velocities or the propulsion forces of the cargo and the JM, the lines are only view guides connecting the data points.

B. Moving Cargo

In the earlier subsection V A, the cargo was held stationary thereby allowing us to determine the motion of the JM by looking only at the propulsion forces. In this subsection, the cargo is allowed to freely move due to the hydrodynamic forces generated by sub-problems 3a and 3b in Figure 3. For the case of $\alpha = \frac{\pi}{2}$, the velocities of the JM (U) and the cargo (V) are presented for a range of values of λ in Figure 10. Here, we see that $U \rightarrow 0.25$ as $e \rightarrow \infty$ as expected with the cargo becoming stationary and the terminal velocity approaching $\frac{1-\cos^2\alpha}{4}$ (JM in an unbounded fluid [36]). As shown in this scenario, for sufficiently small values of α for a given λ , We note that the relative velocity between the two spheres reduces ($U \rightarrow V$) as $e \rightarrow 0$. However, note that the propulsion component of the forces (i.e. F^c from the third sub-problem 3c) does not include the lubrication effects from the hydrodynamic drag. Thus, the relative velocity (however small) between the two spheres provides the lubrication forces to counter the increasing propulsion forces on the two spheres towards each other. In such a scenario, the JM and the cargo approach a constant "towing" velocity in the limit of making contact with each other.

The solutions to the velocities of the JM and the cargo for different stagnant cap sizes of the JM for a size ratio $\lambda = 5$ are presented in Figure 11. Note, the corresponding propulsion forces were shown in Figure 8. In these cases, the values of α are sufficiently large to allow enough solute accumulation such that the JM and the cargo exhibit a reversal in direction of motion. The insets also show that for each value of α there exists a corresponding separation

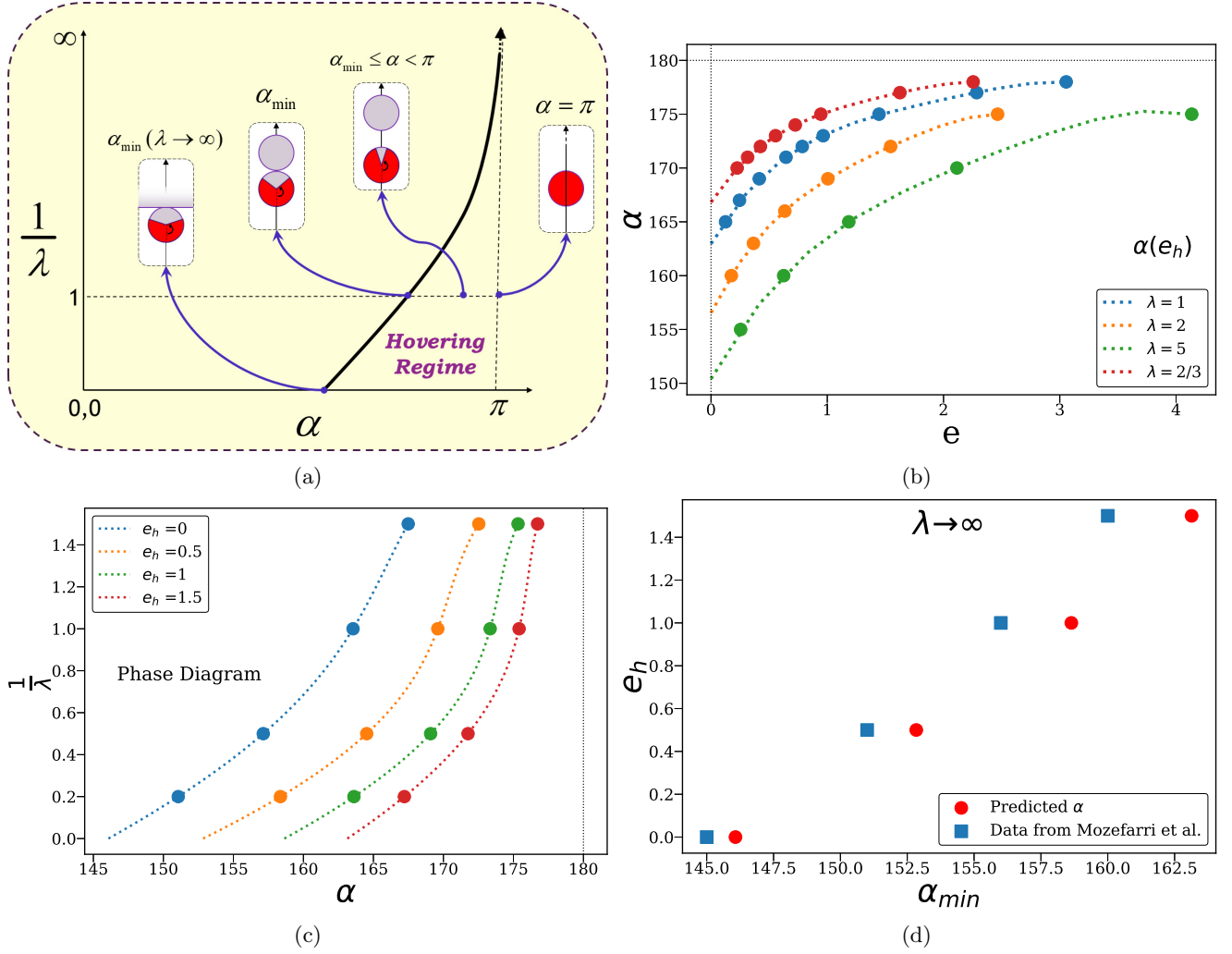


FIG. 9: (a) Illustration of the phase boundary of configurations (λ, α) with hovering states. (b) Polynomial fit of α_{\min} as function of e_h for different sizes of the JM and the cargo. (c) Phase diagram estimated from extrapolation data in Figure 9b. (d) Comparison of the extrapolation of Figure 9c to the limit of $\lambda \rightarrow \infty$ with the literature [36].

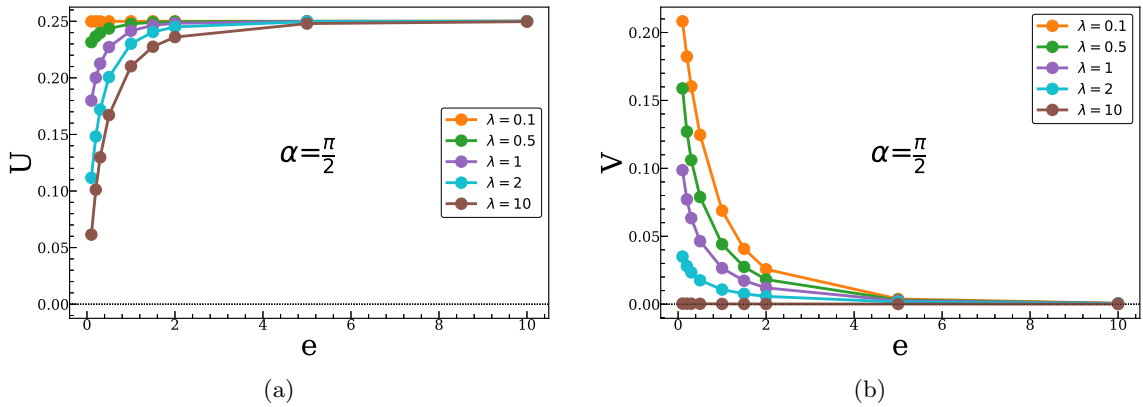


FIG. 10: Velocities for the JM and the cargo for $\alpha = \frac{\pi}{2}$ and a range of values for λ .

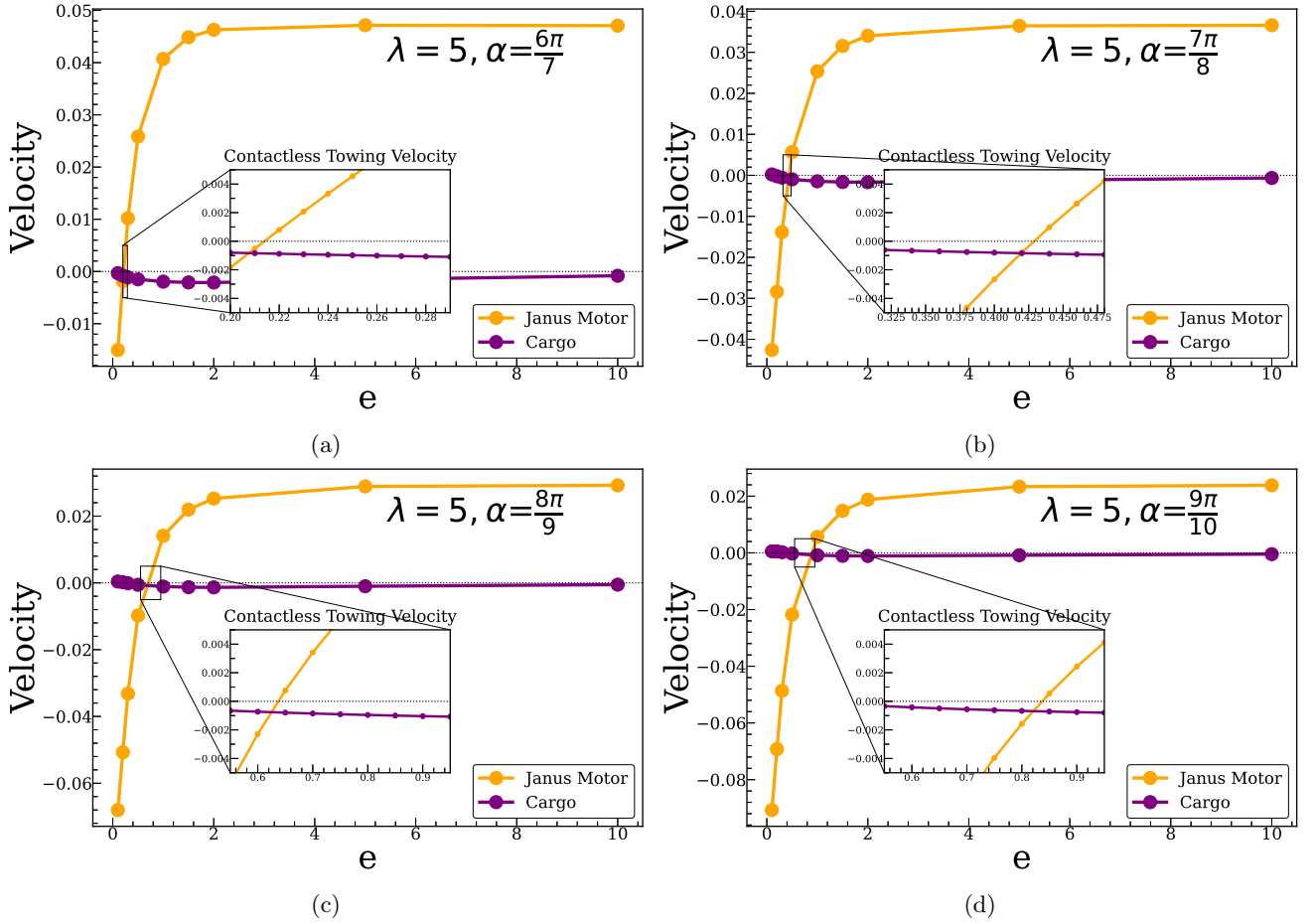


FIG. 11: Plots of the velocities of the JM and a freely moving cargo corresponding to the propulsion forces depicted in Figure 8 for $\lambda = 5$ and different stagnant cap sizes.

distance e_{ct} at which the JM and the cargo have the same velocity. At e_{ct} , the two spheres are able to move in tandem and the motion can be described as a "contactless towing". From these results, this state appears to be stable to axisymmetric perturbations like the state of hovering described in section V A. In general, $e_{ct} \neq e_h$. Furthermore, e_{ct} is also in general different from the separation distance at which the propulsion forces are equal (I.e., $F_J^c = F_C^c$) except for the case of $\lambda = 1$, since the hydrodynamic drags for equal sized spheres moving in tandem are equal [37]. Further investigation will be necessary to develop a phase diagram showing configurations where contactless towing is feasible.

VI. CONCLUSION

We investigated the motion of a JM towards a spherical cargo for different relative ratios λ and for different sizes of the active region on the JM (active cap angle α). We also developed a twin multipole approach for the axisymmetric Stokes stream function using the translation functions developed for the eigenfunctions in terms of Gegenbauer polynomials. When the cargo is held stationary, we discussed the existence of two possible stable steady states along the approach trajectory of the motor. Under select conditions under which the JM comes into a stationary hover at some fixed distance away from the cargo. This state is referred to as the "hovering state". Outside the hovering conditions, the JM continually approaches the cargo to the limit of making contact. When the cargo and the JM are free to move, they can achieve a similar limit of contact and translate together at a steady terminal velocity. This state is referred to as the "towing state". However, under select conditions, the two spheres can translate at a steady terminal velocity at a finite separation distance. We call the latter state "contact less towing state". Finally, we developed a phase diagram based on the qualitative observations of the properties of the hovering regime for the stationary cargo case.

Appendix A: Translational Theorems modified

Using the relationship $g_n(\gamma) = (p_{n+1}(\gamma) - p_{n-1}(\gamma))/(2n+1)$, the eigen functions in 15 can be rewritten as

$$\frac{g_n(\gamma_2)}{r_2^n} = \left(\frac{1}{2n+1} \right) \left(\frac{p_{n+1}(\gamma_2)}{r_2^n} - \frac{p_{n-1}(\gamma_2)}{r_2^n} \right) \quad (\text{A1})$$

$$\frac{g_n(\gamma_2)}{r_2^{n-2}} = \left(\frac{r_2^2}{2n+1} \right) \left(\frac{p_{n+1}(\gamma_2)}{r_2^n} - \frac{p_{n-1}(\gamma_2)}{r_2^n} \right) \quad (\text{A2})$$

Using the translation theorem for the legendre polynomial functions 6, the expressions in A1 and A2 can further be simplified to

$$\frac{g_n(\gamma_2)}{r_2^n} = \left(\frac{1}{2n+1} \right) \left(\frac{r_2^2}{R^{n+2}} \sum_{m=0}^{\infty} \binom{m+n+1}{n+1} \left(\frac{r_1}{R} \right)^m p_m(\gamma_1) - \frac{1}{R^n} \sum_{m=0}^{\infty} \binom{m+n-1}{n-1} \left(\frac{r_1}{R} \right)^m p_m(\gamma_1) \right) \quad (\text{A3})$$

$$\frac{g_n(\gamma_2)}{r_2^{n-2}} = \left(\frac{1}{2n+1} \right) \left(\frac{r_2^4}{R^{n+2}} \sum_{m=0}^{\infty} \binom{m+n+1}{n+1} \left(\frac{r_1}{R} \right)^m p_m(\gamma_1) - \frac{r_2^2}{R^n} \sum_{m=0}^{\infty} \binom{m+n-1}{n-1} \left(\frac{r_1}{R} \right)^m p_m(\gamma_1) \right) \quad (\text{A4})$$

We can expand $r_2^n = (R^2 + r_1^2 - 2Rr_1\gamma_1)^{\frac{n}{2}}$ as follows [38]

$$r_2^n = \sum_{l=0}^n R_{nl}(r_1, R) p_l(\gamma_1) \quad (\text{A5})$$

where $R_{nl}(r_1, R)$ are the radial functions as defined in [38]. The summation in A5 is shown to be finite and to truncate at $l \leq n/2$ for positive, even values of n . Equations A3 and A4 reduce to

$$\frac{g_n(\gamma_2)}{r_2^n} = \left(\frac{1}{2n+1} \right) \left(\sum_{l=0}^1 \sum_{m=0}^{\infty} \frac{R_{2l}(r_1, R)}{R^{n+2}} \binom{m+n+1}{n+1} \left(\frac{r_1}{R} \right)^m p_m(\gamma_1) p_l(\gamma_1) - \sum_{m=0}^{\infty} \frac{1}{R^n} \binom{m+n-1}{n-1} \left(\frac{r_1}{R} \right)^m p_m(\gamma_1) \right) \quad (\text{A6})$$

$$\begin{aligned} \frac{g_n(\gamma_2)}{r_2^{n-2}} &= \left(\frac{1}{2n+1} \right) \left(\sum_{l=0}^2 \sum_{m=0}^{\infty} \frac{R_{4l}(r_1, R)}{R^{n+2}} \binom{m+n+1}{n+1} \left(\frac{r_1}{R} \right)^m p_m(\gamma_1) p_l(\gamma_1) \right) \\ &\quad - \left(\frac{1}{2n+1} \right) \left(\sum_{l=0}^1 \sum_{m=0}^{\infty} \frac{R_{2l}(r_1, R)}{R^n} \binom{m+n-1}{n-1} \left(\frac{r_1}{R} \right)^m p_m(\gamma_1) p_l(\gamma_1) \right). \end{aligned} \quad (\text{A7})$$

noting that $p_0(\gamma) = 1, p_1(\gamma) = \gamma$ and $p_2(\gamma) = (3\gamma^2 - 1)/2$ and using Bonnets recursion theorem, we can linearize the product of the Legendre polynomials in A6 and A7. Finally, grouping coefficients for different orders of the Legendre polynomials, we derive the translation theorem for the Eigen functions given in 16 and 17 with the following definitions for $\Omega_1 - \Omega_8$

$$\Omega_1 = \binom{m+n+1}{n+1} \left(\frac{R_{20}}{R^{m+n+2}} \right) - \binom{m+n-1}{n-1} \left(\frac{1}{R^{m+n}} \right), \quad (\text{A8})$$

$$\Omega_2 = \binom{m+n+1}{n+1} \left(\frac{m}{2m+1} \right) \left(\frac{R_{21}}{R^{m+n+2}} \right), \quad (\text{A9})$$

$$\Omega_3 = \binom{m+n+1}{n+1} \left(\frac{m+1}{2m+1} \right) \left(\frac{R_{21}}{R^{m+n+2}} \right), \quad (\text{A10})$$

$$\Omega_4 = \binom{m+n+1}{n+1} \left(\frac{1}{R^{m+n+2}} \right) \left\{ R_{40} + R_{42} \left[1 - \frac{3}{2} \left(\frac{(m+1)(m+2)}{(2m+1)(2m+3)} + \frac{m(m-1)}{(2m+1)(2m-1)} \right) \right] \right\} - \binom{m+n-1}{n-1} \left(\frac{R_{20}}{R^{m+n}} \right), \quad (\text{A11})$$

$$\Omega_5 = \frac{m}{2m+1} \left[\binom{m+n+1}{n+1} \left(\frac{R_{41}}{R^{m+n+2}} \right) - \binom{m+n-1}{n-1} \left(\frac{R_{21}}{R^{m+n}} \right) \right], \quad (\text{A12})$$

$$\Omega_6 = \frac{m+1}{2m+1} \left[\binom{m+n+1}{n+1} \left(\frac{R_{41}}{R^{m+n+2}} \right) - \binom{m+n-1}{n-1} \left(\frac{R_{21}}{R^{m+n}} \right) \right], \quad (\text{A13})$$

$$\Omega_7 = \frac{3}{2} \left(\frac{(m+1)(m+2)}{(2m+1)(2m+3)} \right) \binom{m+n+1}{n+1} \left(\frac{R_{42}}{R^{m+n+2}} \right), \quad (\text{A14})$$

$$\Omega_8 = \frac{3}{2} \left(\frac{m(m-1)}{(2m+1)(2m-1)} \right) \binom{m+n+1}{n+1} \left(\frac{R_{42}}{R^{m+n+2}} \right), \quad (\text{A15})$$

$$(\text{A16})$$

We can interchange the indices 1, 2 to translate the Eigenfunctions to the second sphere. We note that the final form of the translation theorems 16,17 are valid only along the surfaces of the two spheres and the corresponding values of $R_{ij} \Leftrightarrow R_{ij}(r_1, R)$ for $(i, j) = (2, 0), (2, 1), (4, 0), (4, 1), (4, 2)$. are defined as

$$R_{20}(r_1, R) = R^2 F(-1, -3/2; 3/2; (r_1/R)^2) \quad (\text{A17})$$

$$R_{21}(r_1, R) = -2R^2 \left(\frac{r_1}{R} \right) F(0, -3/2; 5/2; (r_1/R)^2) \quad (\text{A18})$$

$$R_{40}(r_1, R) = R^4 F(-2, -5/2; 3/2; (r_1/R)^2) \quad (\text{A19})$$

$$R_{41}(r_1, R) = -4R^4 \left(\frac{r_1}{R} \right) F(-1, -5/2; 5/2; (r_1/R)^2) \quad (\text{A20})$$

$$R_{42}(r_1, R) = (8/3) R^4 \left(\frac{r_1}{R} \right)^2 F(0, -5/2; 7/2; (r_1/R)^2) \quad (\text{A21})$$

where the function F is Gauss' hypergeometric function defined as

$$F(a, b; c; x) = 1 + \sum_{k=1}^{\infty} \frac{(a)_k (b)_k}{k! (c)_k} (x)^k \quad (\text{A22})$$

with

$$(a)_k = \Gamma(a+k)/\Gamma(a) \quad (\text{A23})$$

	F^{JP}	F^C
Original Size	0.3935	-0.2089
10% Closer Box	0.3936	-0.2087
25% Closer Box	0.3940	-0.2084

TABLE I: We use the case of $\lambda = 1$, $\alpha = \pi/2$, and $R = 2.1$. We show how the box size does not effect convergence. Our forces are all nondimensionalized.

	F^{JP}	F^C
5% Finer Mesh	0.3933	-0.2089
Original Mesh	0.3935	-0.2089
5% Coarser Mesh	0.3927	-0.2089

TABLE II: We use the case of $\lambda = 1$, $\alpha = \pi/2$, and $R = 2.1$. We show how our mesh is already converged. Our forces are all nondimensionalized.

Appendix B: COMSOL

We used COMSOL Multiphysics to collaborate the validity of our diffusiophoretic results. We place our two particles in a large cube ($250R_1 \times 250R_1 \times 250R_1$) to create an infinite medium (more on these dimensions later), with the Janus motor's center corresponding to the cube's center/origin. We define the concentration flux on the surface of the Janus motor (with radius R_1), and its velocity in terms the concentration gradient. We also assign the necessary boundary conditions, including perfect slip on the outer box (not including the inlet or outlet),

$$\mathbf{u} \cdot \mathbf{n}|_{wall} = 0, \quad (B1)$$

$$\mathbf{n} \cdot \boldsymbol{\sigma} \cdot \mathbf{t}|_{wall} = 0. \quad (B2)$$

We assign an inlet, the bottom of the box, with no velocity ($\mathbf{V} = \mathbf{0}$) since there is nothing flowing inward. Our outlet, the top of the box, conditions are

$$\mathbf{n} \cdot \boldsymbol{\sigma} \cdot \mathbf{t}|_{outlet} = 0, \quad (B3)$$

$$\mathbf{n} \cdot \boldsymbol{\sigma} \cdot \mathbf{n}|_{outlet} = 1 \text{ atm}. \quad (B4)$$

For the cargo, we set boundary conditions of no slip ($\mathbf{u} = \mathbf{0}$) and of no flux ($J = 0$). Finally, we set the sides of the box to have no concentration ($C = 0$).

COMSOL then discretizes the volume by tetrahedral mesh and the surfaces by triangles. COMSOL employs the finite element method to solve the concentration and the Stokes equations, by discretizing those equations and solving them using the weak formulation. We choose to have the concentration and velocity solved using quadratic shape functions, while the pressure is solved using linear ones.

To ensure our COMSOL results were themselves converged, we tested the mesh, relative tolerance, and box size. We use the test case of $\lambda = 1$, $\alpha = \pi/2$, and $R = 2.1$ Starting with the box size, we decreased the box on all sides to prove that the box size we used for all of our models ($250R_1 \times 250R_1 \times 250R_1$) returned a converged result. The results of these models can be seen in Table I and show that even for 25% closer wall our forces are within 1% of the original box size. Next we turn to the mesh to ensure that we have small enough elements, given that mesh must be fine when dealing with steep gradients. We prove that our mesh is fine enough, by showing that going both coarser and finer does not make a difference (Table II). Lastly we looked at the relative tolerance. Our original tolerance is 0.0004 (a number decided a priori considered both with the mesh and computation time). We are able to show that our relative tolerance returns a converged result (Table III), and finally prove that our model decisions are all returning accurate and precise results. We see these results of our test case (only using original values for mesh, box size, and tolerance) in our plots when comparing to the twin multipole approach in Figure 12a. We also see the problem where we have hovering in Figure 12b and find that COMSOL is able to capture this hovering behavior as well.

We can also validate the twin sphere solutions by comparing the results for the forces $F_J^a + F_J^b, F_C^a + F_C^b$ to the hydrodynamic drag values for two spheres moving in tandem from tabulated results of the Stimson and Jeffrey

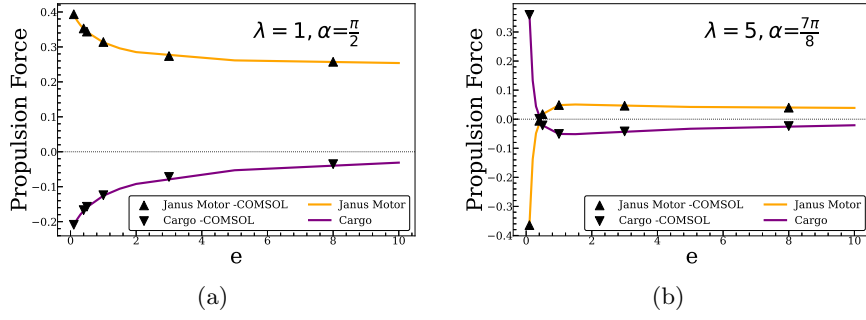


FIG. 12: Two examples, one of hovering and one of towing, of how well the COMSOL results match the twin multipole approach results.

	F^{JP}	F^C
Smaller Tolerance (0.00009)	0.3933	-0.2089
Original Tolerance (0.0004)	0.3933	-0.2089
Larger Tolerance (0.0005)	0.3933	-0.2089

TABLE III: We use the case of $\lambda = 1$, $\alpha = \pi/2$, and $R = 2.1$. We show how our relative tolerance already returns a converged result. Our forces are all nondimensionalized.

solutions (S&J) [37] taken from [39]. The forces (scaled by $-6\pi\mu R_1$) on the Janus motor and the cargo are given by f_1 and f_2 respectively.

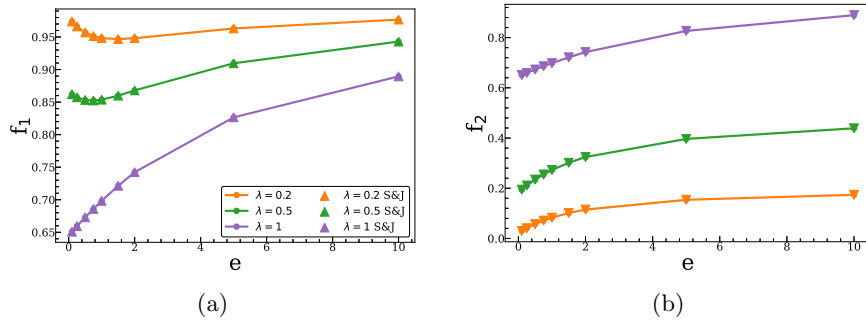


FIG. 13: Validation of the twin multipole approach using the hydrodynamic forces for the Janus motor and the cargo from [39] (S&J).

-
- [1] E. Lauga and T. R. Powers, The hydrodynamics of swimming microorganisms, *Reports on progress in physics* **72**, 096601 (2009).
 - [2] H. Su, C.-A. H. Price, L. Jing, Q. Tian, J. Liu, and K. Qian, Janus particles: design, preparation, and biomedical applications, *Materials today bio* **4**, 100033 (2019).
 - [3] L.-T.-C. Tran, S. Lesieur, and V. Faivre, Janus nanoparticles: materials, preparation and recent advances in drug delivery, *Expert opinion on drug delivery* **11**, 1061 (2014).
 - [4] D. Ho, X. Sun, and S. Sun, Monodisperse magnetic nanoparticles for theranostic applications, *Accounts of chemical research* **44**, 875 (2011).
 - [5] A. Walther and A. H. Muller, Janus particles: synthesis, self-assembly, physical properties, and applications, *Chemical reviews* **113**, 5194 (2013).
 - [6] E. M. Purcell, Life at low reynolds number, *American journal of physics* **45**, 3 (1977).
 - [7] J. L. Anderson and D. C. Prieve, Diffusiophoresis: Migration of colloidal particles in gradients of solute concentration, *Separation and Purification Methods* **13**, 67 (1984).
 - [8] J. L. Anderson, Colloid transport by interfacial forces, *Annual review of fluid mechanics* **21**, 61 (1989).
 - [9] R. Golestanian, T. B. Liverpool, and A. Ajdari, Propulsion of a molecular machine by asymmetric distribution of reaction products, *Physical review letters* **94**, 220801 (2005).
 - [10] J. R. Howse, R. A. Jones, A. J. Ryan, T. Gough, R. Vafabakhsh, and R. Golestanian, Self-motile colloidal particles: from directed propulsion to random walk, *Physical review letters* **99**, 048102 (2007).
 - [11] S. J. Ebbens and J. R. Howse, Direct observation of the direction of motion for spherical catalytic swimmers, *Langmuir* **27**, 12293 (2011).
 - [12] S. Ebbens, M.-H. Tu, J. R. Howse, and R. Golestanian, Size dependence of the propulsion velocity for catalytic janus-sphere swimmers, *Physical Review E* **85**, 020401 (2012).
 - [13] X. Zheng, B. Ten Hagen, A. Kaiser, M. Wu, H. Cui, Z. Silber-Li, and H. Löwen, Non-gaussian statistics for the motion of self-propelled janus particles: Experiment versus theory, *Physical Review E* **88**, 032304 (2013).
 - [14] W. F. Paxton, K. C. Kistler, C. C. Olmeda, A. Sen, S. K. St. Angelo, Y. Cao, T. E. Mallouk, P. E. Lammert, and V. H. Crespi, Catalytic nanomotors: autonomous movement of striped nanorods, *Journal of the American Chemical Society* **126**, 13424 (2004).
 - [15] N. Sharifi-Mood, J. Koplik, and C. Maldarelli, Diffusiophoretic self-propulsion of colloids driven by a surface reaction: the sub-micron particle regime for exponential and van der waals interactions, *Physics of Fluids* **25**, 012001 (2013).
 - [16] M. N. Popescu, W. E. Uspal, and S. Dietrich, Self-diffusiophoresis of chemically active colloids, *The European Physical Journal Special Topics* **225**, 2189 (2016).
 - [17] J. F. Brady, Particle motion driven by solute gradients with application to autonomous motion: continuum and colloidal perspectives, *Journal of Fluid Mechanics* **667**, 216 (2011).
 - [18] S. J. Ebbens and J. R. Howse, In pursuit of propulsion at the nanoscale, *Soft Matter* **6**, 726 (2010).
 - [19] W. Wang, W. Duan, S. Ahmed, T. E. Mallouk, and A. Sen, Small power: Autonomous nano-and micromotors propelled by self-generated gradients, *Nano Today* **8**, 531 (2013).
 - [20] R. Kapral, Perspective: Nanomotors without moving parts that propel themselves in solution, *The Journal of Chemical Physics* **138**, 020901 (2013).
 - [21] J. L. Moran and J. D. Posner, Phoretic self-propulsion, *Annual Review of Fluid Mechanics* **49**, 511 (2017).
 - [22] L. Baraban, D. Makarov, R. Streubel, I. Monch, D. Grimm, S. Sanchez, and O. G. Schmidt, Catalytic janus motors on microfluidic chip: deterministic motion for targeted cargo delivery, *ACS nano* **6**, 3383 (2012).
 - [23] L. Baraban, M. Tasinkevych, M. N. Popescu, S. Sanchez, S. Dietrich, and O. Schmidt, Transport of cargo by catalytic janus micro-motors, *Soft Matter* **8**, 48 (2012).
 - [24] P. Bayati and A. Najafi, Dynamics of two interacting active janus particles, *The Journal of chemical physics* **144**, 134901 (2016).
 - [25] B. Nasouri and R. Golestanian, Exact axisymmetric interaction of phoretically active janus particles, *Journal of Fluid Mechanics* **905** (2020).
 - [26] F. Rojas-Pérez, B. Delmotte, and S. Michelin, Hydrochemical interactions of phoretic particles: a regularized multipole framework, *Journal of Fluid Mechanics* **919** (2021).
 - [27] N. Sharifi-Mood, A. Mozaffari, and U. M. Córdova-Figueroa, Pair interaction of catalytically active colloids: from assembly to escape, *Journal of Fluid Mechanics* **798**, 910 (2016).
 - [28] J. Happel and H. Brenner, *Low Reynolds number hydrodynamics: with special applications to particulate media*, Vol. 1 (Springer Science & Business Media, 2012).
 - [29] M. Teubner, The motion of charged colloidal particles in electric fields, *The Journal of Chemical Physics* **76**, 5564 (1982).
 - [30] S. Lee and L. Leal, Motion of a sphere in the presence of a plane interface. part 2. an exact solution in bipolar co-ordinates, *Journal of Fluid Mechanics* **98**, 193 (1980).
 - [31] D. Ross, The potential due to two point charges each at the centre of a spherical cavity and embedded in a dielectric medium, *Australian Journal of Physics* **21**, 817 (1968).
 - [32] D. J. Jeffrey, Conduction through a random suspension of spheres, *Proceedings of the Royal Society of London. A. Mathematical and Physical Sciences* **335**, 355 (1973).
 - [33] D. Jeffrey and Y. Onishi, Calculation of the resistance and mobility functions for two unequal rigid spheres in low-reynolds-

- number flow, *Journal of Fluid Mechanics* **139**, 261 (1984).
- [34] L. G. Leal, *Advanced transport phenomena: fluid mechanics and convective transport processes*, Vol. 7 (Cambridge university press, 2007).
- [35] S. Kim and S. J. Karrila, *Microhydrodynamics: principles and selected applications* (Courier Corporation, 2013).
- [36] A. Mozaffari, N. Sharifi-Mood, J. Koplik, and C. Maldarelli, Self-diffusiophoretic colloidal propulsion near a solid boundary, *Physics of Fluids* **28** (2016).
- [37] M. Stimson and G. B. Jeffery, The motion of two spheres in a viscous fluid, *Proceedings of the Royal Society of London. Series A, Containing Papers of a Mathematical and Physical Character* **111**, 110 (1926).
- [38] R. Sack, Generalization of laplace's expansion to arbitrary powers and functions of the distance between two points, *Journal of Mathematical Physics* **5**, 245 (1964).
- [39] M. Cooley and M. O'neill, On the slow motion of two spheres in contact along their line of centres through a viscous fluid, in *Mathematical Proceedings of the Cambridge Philosophical Society*, Vol. 66 (Cambridge University Press, 1969) pp. 407–415.